https://doi.org/10.1590/jatm.v18.1417 ORIGINAL PAPER

Lunar Regolith Classification Using Discrete Element Method on Single-Deck Vibrating Screen

Pedro Cáceres[1], Alejandro Lopez-Telgie[1], Cristian G. Rodríguez[1], Cristián Vicuña[1], Manuel Moncada M.[1,*]

1.University of Concepción – Faculty of Engineering – Department of Mechanical Engineering – Concepción – Chile.

*Corresponding author: manuelmoncada@udec.cl

ABSTRACT

The sustainable use of lunar resources requires efficient processing of lunar regolith, particularly for advanced manufacturing techniques such as selective laser melting and laser engineered net shaping, which demand particles ≤ 100 µm. This research employs the discrete element method (DEM) to simulate a vibrating screen operating in the Moon's environment, specifically investigating and providing insights into the effects of vibration parameters and screen inclination on screening efficiency, reaching a maximum efficiency of 76.9%. Additionally, the study explores the feasibility of transporting a vibrating screen from Earth to the Moon, considering its mass and the actual capabilities of the Space Launch System Block 1 Cargo, concluding that the screen can be transported to the Moon. Although the simulated efficiency is over 70%, better results are likely achievable by studying other configurations of motion or different geometries for the screen and deck. This work represents the first DEM-based study of vibrating screens under lunar gravity and provides essential insights for *in situ* resource utilization strategies.

Keywords: Vibrating screen; Discrete element method; Lunar gravitational environment.

INTRODUCTION

The colonization of the Moon represents the next stage in space exploration due to its practical advantages for future missions to Mars and beyond. The Moon's lower gravity facilitates spacecraft launches for these missions. Recently, diverse projects such as Luna, Kaguya, Chang'e, and Artemis (Li *et al.* 2021; Pickrell 2022) have aimed to explore and eventually colonize the Moon. These projects have enabled researchers to analyze lunar regolith and Moon rock samples and conduct studies from lunar orbit to understand the composition and characteristics of the Moon's surface (Otto *et al.* 2018).

In situ resource utilization (ISRU) is required to establish colonies on the Moon, facilitating the manufacture of habitats and tools by reducing the need to transport raw materials from Earth (Sanders and Larson 2013). This process is extremely costly, making ISRU essential. The primary focus of the studies on Moon resources is the lunar regolith, intended to be used as raw material for buildings and energy generation in lunar colonies. The Moon's regolith is a fine, dust-like material found all over the Moon's surface, with various compounds, including basalts, anorthites, and small traces of thorium, rare earth elements, and helium-3 (Crawford 2015).

Among the known manufacturing processes applicable on Earth, only a few have been proven feasible for use on the Moon. Notably, selective laser melting and laser engineered net shaping can directly utilize regolith as feedstock, requiring particle sizes of 50 µm and 100 µm, respectively (Isachenkov *et al.* 2021). The size distribution of regolith varies from units of micrometers to up to 10 millimeters, with a mean of around 40 to 60 µm, depending on the sample considered (Otto *et al.* 2018). This size

Received: Oct. 15, 2024 | **Accepted:** Nov. 06, 2025
Peer Review History: Single Blind Peer Review.
Section editor: Renato Reboucas de Medeiros

distribution results from millions of years of bombardment by asteroids, meteorites, and micrometeorites on the satellite's surface. Due to these impacts, the regolith can contain vitreous agglutinates among the particles in forms not seen anywhere on Earth, which also influence the size distribution of the Moon dust. The shape of the particles is highly non-spherical, as they have not been subject to the erosive agents that can be encountered on Earth, such as wind and water currents, resulting in amorphous grains with variable but generally high porosity (McKay *et al.* 1991).

As the manufacturing processes require a maximum of 100 μm, efficient classification of regolith is a critical challenge. Among the alternatives for size classification are the system proposed by Adachi *et al.* (2017), based on the electrostatic traveling wave to separate particles less than 20 μm in diameter, and a centrifugal sieve proposed by Dreyer *et al.* (2012) that circumvents the issue of low gravity. However, no systematic comparison exists between these methods, and vibrating screens were chosen due to their extensive use in size separation in mineral processing on Earth. This enables comparisons between well-studied Earth systems and their potential performance on the Moon.

Due to the discrete nature of the problem, the sieving process is analyzed through the discrete element method (DEM), initially proposed by Cundall and Strack (1979). The use of DEM in mineral processing on Earth has been widely adopted and validated (Toledo *et al.* 2025), and its use in the modeling of granular flows under microgravity has been successfully validated by Ozaki (2023) using an artificial gravity generator at the International Space Station. One limitation that could affect the DEM modeling of the system in the lunar environment is the lack of parameter calibration, which could impact the model's accuracy (Coetzee 2019).

Li *et al.* (2023) have previously conducted a study with a similar objective, aiming for particles with a maximum sieve size of 2 mm to extract oxygen and utilizing a double mesh vibrating screen. In their study, they provide experimental validation was provided for the utilization of DEM in microgravity by simulating the Moon's gravitational attraction with a magnetic field for comparing the motion of a single particle with results obtained in the same situation within a DEM computational environment, with successful results, establishing precedents for future investigations on the sieving of regolith.

This paper presents a DEM-based numerical model of a vibrating screen operating under lunar gravity. The goal is to identify how key operational parameters (inclination, amplitude, and frequency) affect screening efficiency and to compare the results directly with Earth conditions. This provides new insights into how reduced gravity modifies stratification and particle passage. In addition, a preliminary feasibility assessment of screen transport to the Moon is included. Finally, it is emphasized that this work does not include direct experimental validation, which is currently infeasible under actual lunar conditions, and it is considered that the expense (economic and environmental) of microgravity experimentation on Earth is not justified under the current state of the art. Instead, it is argued that numerical simulations such as DEM should be the first step, followed by physical experimentation in terrestrial microgravity facilities.

Mathematical model

The model was developed using the DEM. The following subsections summarize the governing equations of motion and the adopted contact models.

Equations of motion

The equation governing the motion of any given particle *i* is defined as presented in vectorial Eqs. 1 and 2:

$$m_i \frac{\mathrm{d}\boldsymbol{v}_i}{\mathrm{d}t} = m_i \boldsymbol{g} + \sum_{j=1}^{N} \boldsymbol{F}_{ij} \tag{1}$$

$$I_i \frac{\mathrm{d}\boldsymbol{\omega}_i}{\mathrm{d}t} = \sum_{j=1}^{N} \boldsymbol{M}_{ij} \tag{2}$$

where, for the given *i* particle, m_i is its mass, v_i its velocity, I_i its moment of inertia, ω_i its angular velocity, g is the gravity to which the system of particles is subject, and, lastly, F_{ij} and M_{ij} are the force and moment produced by the contact with other particles or by boundary collisions.

Contact model

The normal force contact model utilized in this study is the hysteretic linear spring model proposed by Walton and Braun (1986), defined in Eqs. 3 and 4:

$$F_{n,j} = \begin{cases} \min\left(K_{nl} \cdot s_n^t \, , F_n^{t-\Delta t} + K_{nu} \cdot \Delta s_n\right), \text{if } \Delta s_n \geq 0 \\ \max\left(F_n^{t-\Delta t} + K_{nu} \cdot \Delta s_n \, , \lambda \cdot K_{nl} \cdot s_n^t\right), if \ \Delta s_n < 0 \end{cases} \tag{3}$$

$$\Delta s_n = s_n^t - s_n^{t-\Delta t} \tag{4}$$

where F_n^t y $F_n^{t-\Delta t}$ are the elastoplastic contact forces at points t and $t - \Delta t$, respectively; Δt is the time step; Δs_n is the change in particle overlap, calculated from the particles' geometric centers in the case of spherical particles, and assumed positive when particles are approaching each other; s_n^t and $s_n^{t-\Delta t}$ are the particle overlaps at points t and $t - \Delta t$; K_{nl} and K_{nu} are the values of contact stiffness for loading and unloading cases, which are calculated from the Young's modulus as defined by ESSS (2020) in the Rocky DEM user manual; λ is a dimensionless constant, whose value for the utilized software is 0.001.

For the tangential contact force, a linear spring model with Coulomb limit was applied, as defined in Eqs. 5-7, where F_τ^t and $F_\tau^{t-\Delta t}$ are the tangential contact forces for temporal points t and $t - \Delta t$; μ is the coefficient of friction; $\Delta s\tau$ is the relative tangential displacement of the particles for two consecutive time points; r_k is the tangential stiffness ratio, defined in this case as 1:

$$F_\tau^t = min\left(|F_\tau{}'|, \mu F_{n,j}\right) \frac{F_\tau{}'}{|F_\tau{}'|} \tag{5}$$

$$F_{\tau,e}^t = F_\tau^{t-\Delta t} - K_\tau \Delta s_\tau \tag{6}$$

$$K_\tau = r_K K_{nl} \tag{7}$$

The rolling resistance model is defined in Eq. 8, and it is used to represent the moment effect on particles that deviate from perfect spheres and are subject to rotation:

$$\boldsymbol{M}_r = -\mu_r \, |r| \, F_n \frac{\boldsymbol{\omega}}{|\boldsymbol{\omega}|} \tag{8}$$

In this equation, M_r is the moment on the studied particle, μ_r is the rolling resistance coefficient, F_n is the normal contact force, and ω is the angular velocity of the particle.

METHODOLOGY

In this study, the motion of the screen meshes was simulated using the validated DEM under Moon gravity conditions. The first phase of the study involved the simulation of an existing model of a vibrating screen, similar to the one used by Moncada

and Rodríguez (2018), with a continuous feed of particles with a size distribution that allows the presence of a bottom, middle, and top flows in the screen.

The screen operation was configured with different values of vibration amplitude, frequency, and screen inclination, in a similar approach to the study conducted by Aghlmandi *et al.* (2018). The objective of this series of cases was to gain insights into the effects of these variables on the efficiency of the screening process in the lunar environment, with the definition of efficiency in Eq. 9, where u is undersized in underflow and f is undersized in feed:

$$E = \frac{\dot{m}_u}{\dot{m}_f} \tag{9}$$

To evaluate the impact of gravity, every motion configuration was applied under Earth and Moon gravity to assess efficiency differences. The values of the three magnitudes mentioned above are presented in Table 1, with four different values for every variable case, which combined represent the motion configurations for the screen on Earth and the Moon. These values correspond to typical operational ranges for terrestrial vibrating screens (Aghlmandi *et al.* 2018; Moncada and Rodríguez 2018; Toledo *et al.* 2025).

Table 1. Operational parameters of the studied cases.

Case	Amplitude [mm]	Frequency [Hz]	Inclination [°]
Variable amplitude	2-4	15	15
Variable frequency	4	15-30	15
Variable inclination	5	20	5-20

Source: Elaborated by the authors.

The particle size distribution (PSD) for the spherical particles is listed below in Table 2.

Table 2. PSD for the analysis of the three variables.

Particle size [mm]	Cumulative percentage [%]
30	100
20	75
11	25

Source: Elaborated by the authors.

The simulation parameters associated with the interaction between elements, material properties, and time are listed in Table 3. The Young's modulus of the boundaries was reduced from 210 GPa to 5 MPa to speed up the simulation times. This approach, widely used in DEM (Lommen *et al.* 2014), preserves bulk flow behavior while accelerating computation. Although this softening may slightly affect contact dynamics, prior sensitivity studies confirm that screening efficiency trends remain valid.

The single-mesh lunar screen was designed in Autodesk Inventor based on ASTM E11 No. 140 (106 μm) dimensions and implemented in Rocky DEM (Fig. 1). The length of the screen deck is 40 mm, and the width is 20 mm, with a rectangular inlet at the upper end of the screen. To reduce computational demand, only one quarter of the mesh was modeled with periodic side boundaries.

Table 3. Simulation parameters for the double deck screen (Otto *et al.* 2018).

Parameter	Value
Simulation time	120 s
Time step	$3 \cdot 10^{-7}$ s
Feed rate	20 t·h
Particles density	2,997.68 kg/m^3
Particles' Young's modulus	5 MPa
Boundaries Young's modulus	5 MPa
Particles' Poisson's ratio	0.3
Particles count	148,648
Rolling resistance	0.7
Static particle – particle friction coefficient	0.3
Static particle – boundary friction coefficient	0.465

Source: Elaborated by the authors.

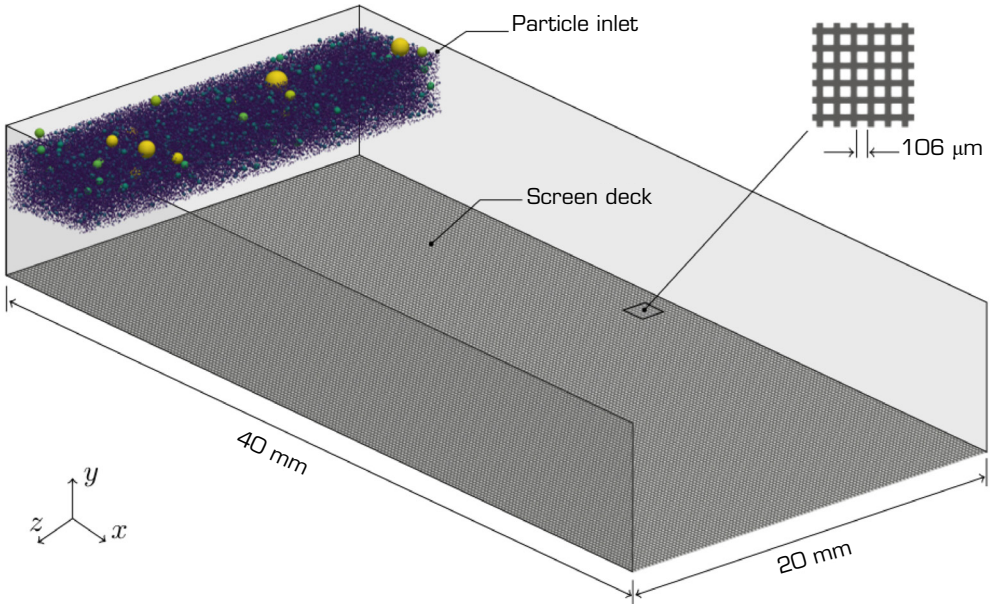

Source: Elaborated by the authors.

Figure 1. Setup of the vibrating screen simulation with ASTM E11 No. 140 mesh.

The configuration for the movement of the screen was based on the results of the double-deck vibrating screen, aiming to obtain a similar Throwing Index K_v (He and Liu 2009), which was calculated with Eq. 10 to match Earth-based optimal configurations, and then varied to explore lunar performance:

$$K_v = \frac{A\omega^2}{g\cos(\alpha)} \tag{10}$$

The applied motion configurations are presented in Table 4, while in Table 5, the mechanical and interaction parameters implemented are listed, based on the study conducted by Otto *et al.* (2018).

Table 4. Motion configuration for ASTM E11 screen.

Variable	Configuration 1	Configuration 2	Configuration 3	Configuration 4
Amplitude [mm]	1.5	1.0	1.5	0.5
Frequency [Hz]	10	15	15	15
Inclination [°]	2.5	2.5	2.5	2.5
Gravity acceleration [m/s2]	1.62	1.62	1.62	1.62
Throwing Index	3.66	5.49	8.23	2.74

Source: Elaborated by the authors.

Table 5. Material parameters for ASTM E11 screen.

Parameter	Value
Simulation time	12 s
Sample frequency	50 Hz
Time step	$3{\cdot}10^{-7}$ s
Feed rate	90 g·h
Particles density	2,997.68 kg·m^3
Particles' Young's modulus	5 MPa
Particles' Poisson's ratio	0.3
Particles count	9,967,337
Rolling resistance	0.7
Static particle – particle friction coefficient	0.3
Static particle – boundary friction coefficient	0.465

Source: Elaborated by the authors.

As for the size distribution of the regolith particles, the sample JSC-1A (Otto *et al.* 2018) was selected, and based on this sample, the following values for cumulative percentage were applied in the Rocky DEM, as seen in Table 6.

Table 6. PSD based on JSC-1A sample.

Particle size [mm]	Cumulative percentage [%]
1.00	100
0.28	90
0.20	80
0.15	70
0.10	55
0.09	50
0.04	28

Source: Elaborated by the authors.

Finally, a preliminary estimation of the vibrating screen mass was performed using data from manufacturers of industrial vibrating screens. This estimate excludes structural supports, actuators, and auxiliary systems and therefore should be considered conservative. The intent was not to propose a complete engineering design but to test order-of-magnitude feasibility for lunar deployment. Then, transport feasibility was assessed with the calculated mass using the ideal rocket equation.

It is important to note that several simplifications were applied in the DEM modeling of the vibrating screen under lunar conditions. In particular, temperature variations and their effects on material properties were neglected, as were electrostatic interactions, which are known to influence fine regolith but are beyond the present study's scope. Particle breakage and cohesion

were not included, and the model assumes constant gravity without local variations. While limiting full physical fidelity, these assumptions are consistent with previous DEM-based studies and allow the isolation of the influence of screen motion and reduced gravity on sieving efficiency.

RESULTS

The efficiency of the double deck screen at different inclination angles is presented in Fig. 2, calculated with Eq. 9. In addition, the PSD of both middle and upper flow is shown in Fig. 3 for operation on the Moon, and in Fig. 4 for operation on the Earth.

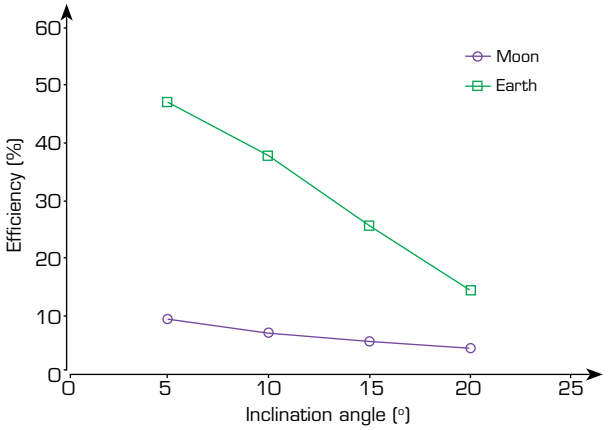

Source: Elaborated by the authors.

Figure 2. Screening efficiency by inclination angle.

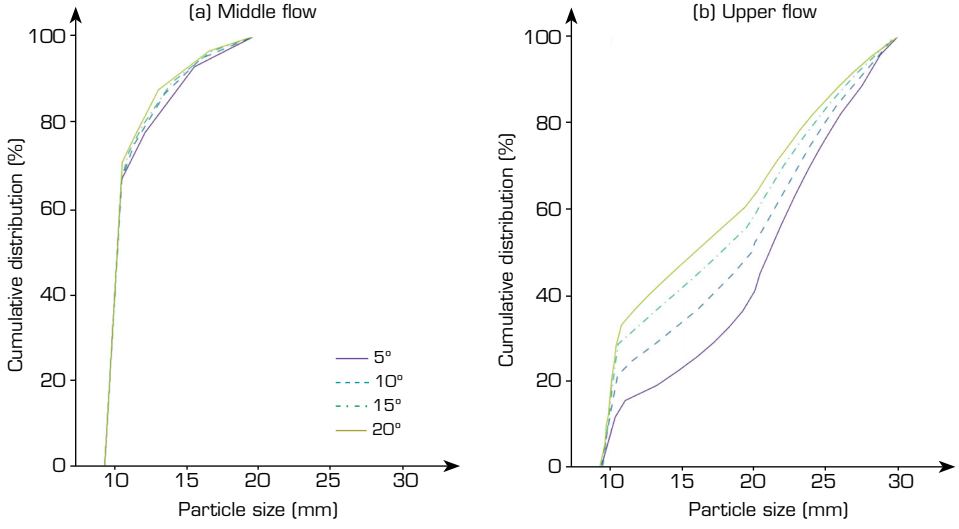

Source: Elaborated by the authors.

Figure 3. PSD on the Moon by inclination angle. (a) Middle; (b) Upper flow.

While on Earth, the inclination angle significantly impacts screening efficiency, as Fig. 2 shows, the effect is notably reduced under lunar gravity. This suggests that lower inclination angles may be required for proper operation on the Moon, or that this variable exerts only a minor influence on efficiency in reduced gravity. On the other hand, as seen in the PSD of the upper flow in both cases, a lower inclination angle implies coarser grains in the exhaust, which is desirable.

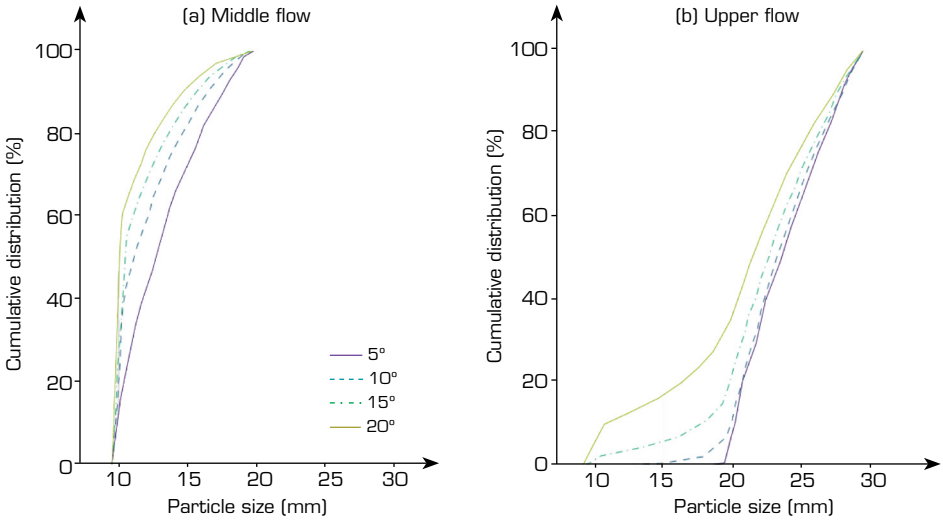

Source: Elaborated by the authors.

Figure 4. PSD on Earth by inclination angle. (a) Middle; (b) Upper flow.

For the case of variable vibration frequency, the screening efficiency on Earth and the Moon is presented in Fig. 5, while the PSD of the middle and upper flow on the Moon is presented in Figs. 6 and 7 for Earth conditions.

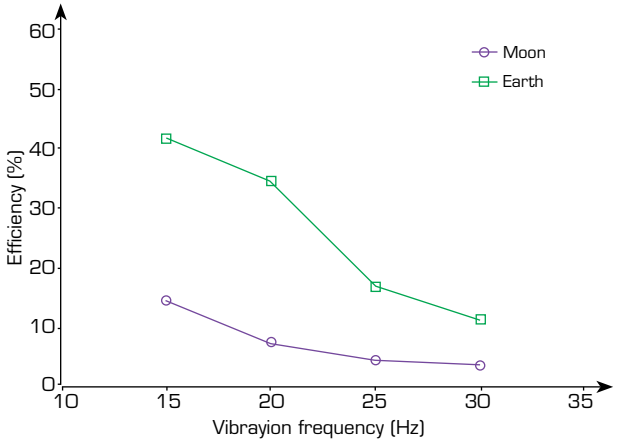

Source: Elaborated by the authors.

Figure 5. Screening efficiency by vibration frequency.

This case, similarly to the previous one, shows an inverse relationship between vibration frequency and screening efficiency. However, this time, the effect of the lower frequencies is stronger than in the inclination case. Thus, lower values for frequency are preferred, although excessively low frequencies could reduce particle residence time, potentially decreasing throughput efficiency.

For the case of vibration amplitude, its effect on efficiency is shown in Fig. 8, while the PSD for the middle and upper flow is shown in Fig. 9 for Moon conditions and Fig. 10 for Earth conditions.

In this case, for the lowest amplitude simulated, the screening efficiency on the Moon is higher than the corresponding Earth case, and results suggest that lower amplitudes may further improve efficiency under lunar gravity. This trend appears opposite to common Earth-based expectations but can be explained by increased particle stratification time in low gravity, compensating for the reduced throwing intensity. The effect on the PSD of both flows on the Moon is similar to the effect of the previously studied variables.

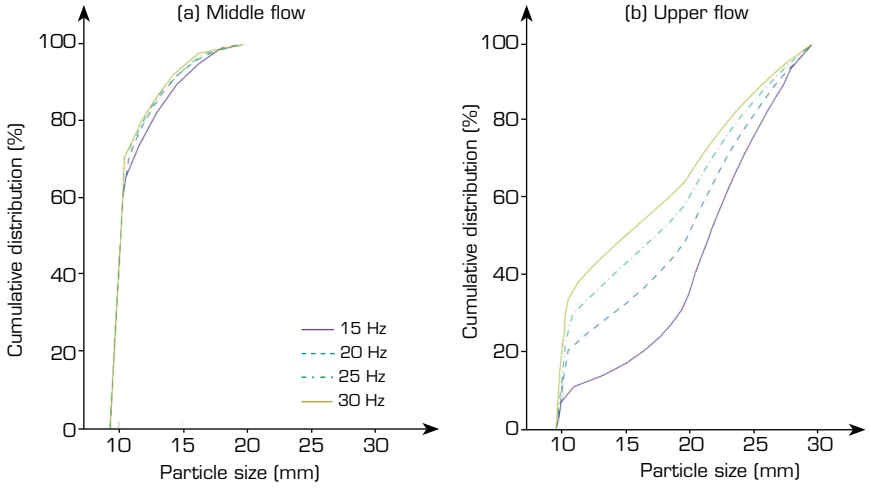

Source: Elaborated by the authors.

Figure 6. PSD on the Moon by vibration frequency. (a) Middle; (b) Upper flow.

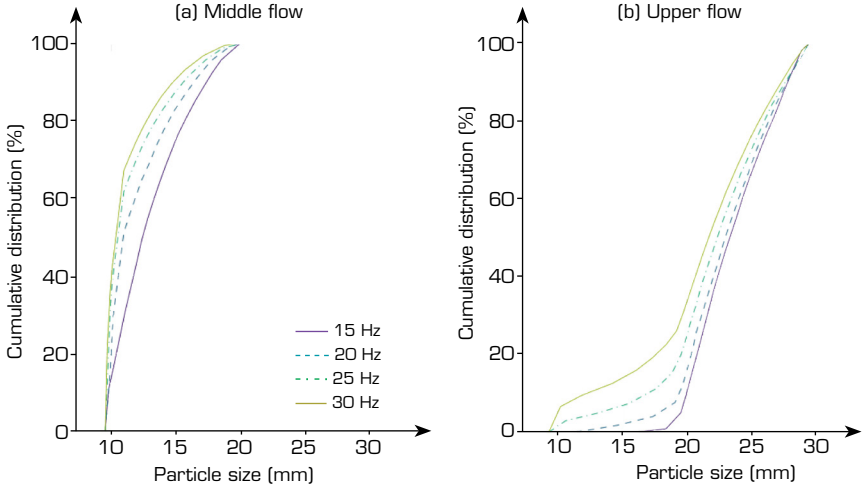

Source: Elaborated by the authors.

Figure 7. PSD on Earth by vibration frequency. (a) Middle; (b) Upper flow.

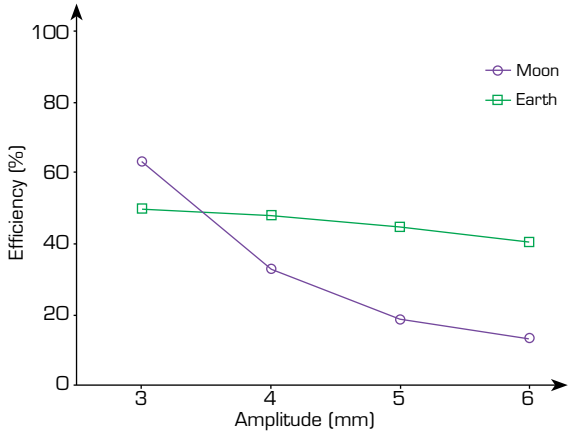

Source: Elaborated by the authors.

Figure 8. Screening efficiency by vibration amplitude.

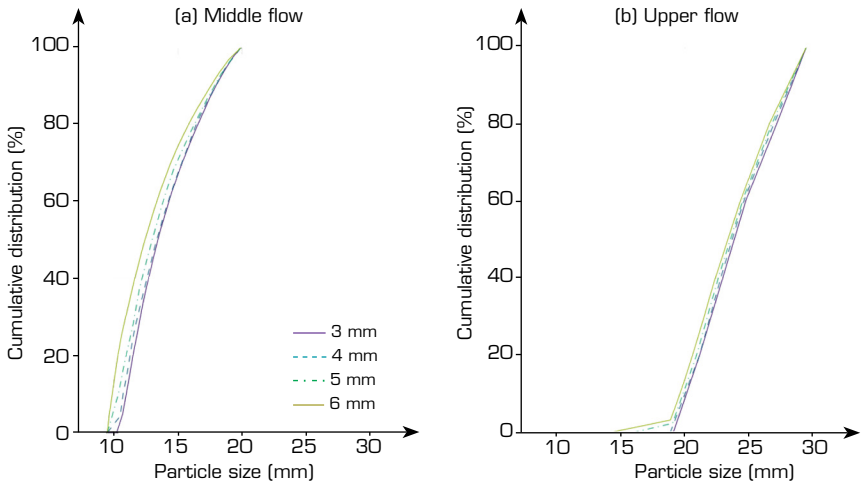

Source: Elaborated by the authors.

Figure 9. PSD on the Moon by vibration amplitude. (a) Middle; (b) Upper flow.

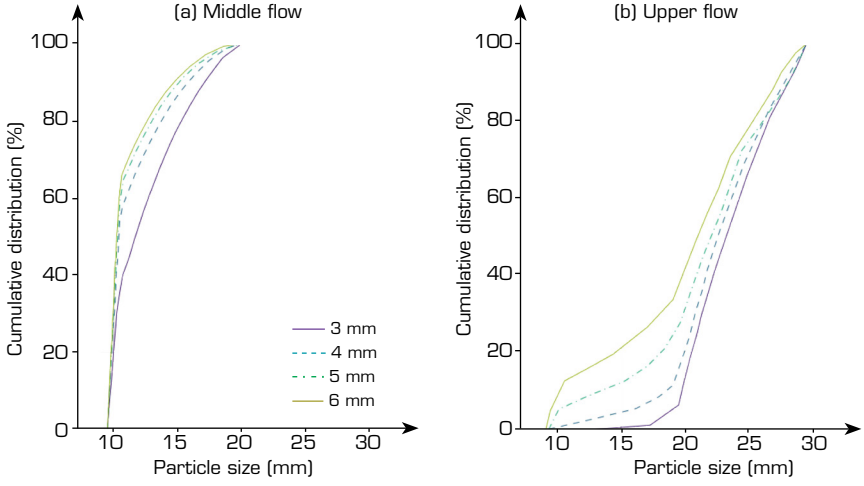

Source: Elaborated by the authors.

Figure 10. PSD on Earth by vibration amplitude. (a) Middle; (b) Upper flow.

For the study on the ASTM E11 screen, with the motion configurations displayed in Table 4 and the simulation parameters of Table 5, the obtained efficiency is shown in Table 7. A graphic representation of the simulated process is provided in Fig. 11.

Table 7. Efficiency of the DEM simulations of the vibrating screen in Moon conditions at different configurations.

Case	Obtained efficiency
Configuration 1	0.507
Configuration 2	0.509
Configuration 3	0.564
Configuration 4	0.640

Source: Elaborated by the authors.

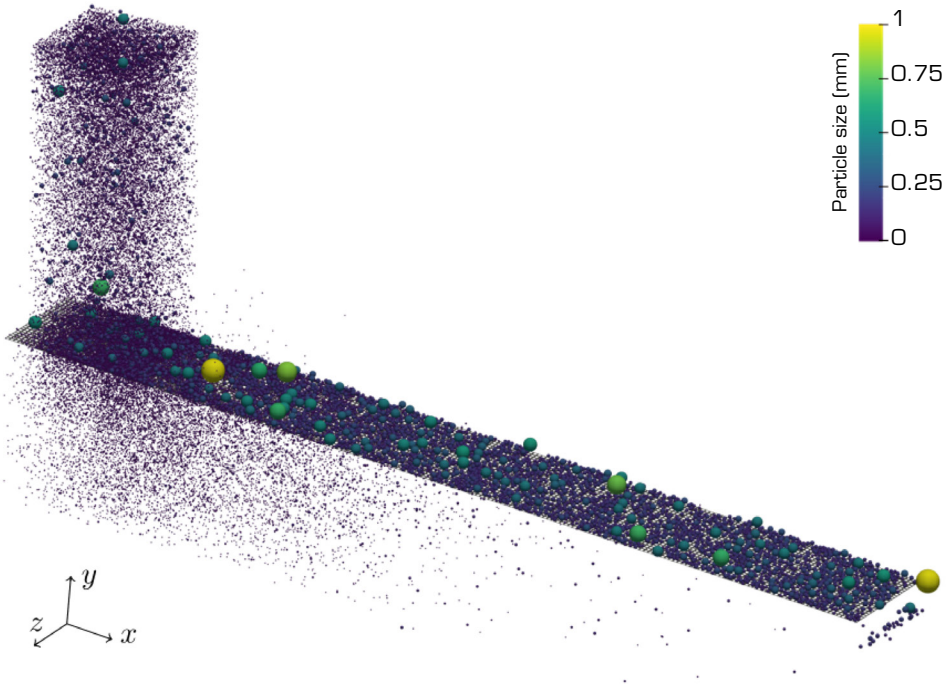

Source: Elaborated by the authors.

Figure 11. Simulation process of the regolith on the ASTM E11 screen.

Among the previous motion configurations, the one with the highest efficiency was selected to analyze screening efficiency as a function of screen length. Table 8 presents the results, starting from a screen length of 10 mm up to 50 mm and including the 200 mm total length of the screen, together with the corresponding efficiency values. This analysis approximates the optimal effective length of the screen mesh.

Table 8. Screen length and respective efficiency.

Screen length	Efficiency	Screen length	Efficiency
10 mm	0.544	40 mm	0.637
20 mm	0.617	50 mm	0.638
30 mm	0.632	200 mm	0.640

Source: Elaborated by the authors.

Based on the previous results, two new simulations, denoted as configurations 5 and 6, were performed with a mesh length of 40 mm, as longer lengths provide less than a 0.5% increase in efficiency. The feed rate was increased to 1 kg·h, and the width of the mesh was increased to 5 mm. The motion configuration for these last two simulations is shown in Table 9.

Table 9. Additional configurations of motion.

Configuration	Amplitude [mm]	Frequency [Hz]	Inclination [°]	Efficiency [%]
5	0.5	15	5	76.9
6	0.2	15	5	61.6

Source: Elaborated by the authors.

For the estimation of the total mass of the vibrating screen, a length of 40 mm was chosen based on the previous results; a feed rate of 22.5 ton·h was considered, leading to a screen of 4.5 m². Thus, following the interpolation curve for nominal data of different industrial vibrating screens presented in Fig. 12, the screen was estimated to have a total mass of approximately 5.14 tons.

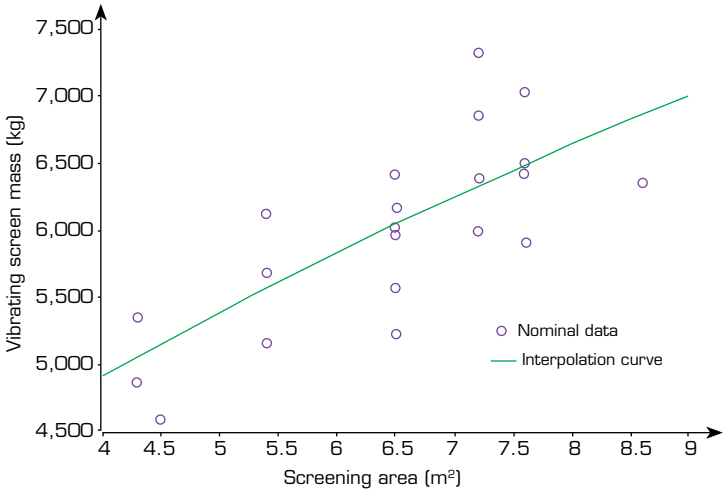

Source: Elaborated by the authors.

Figure 12. Interpolation curve of the known vibrating screen area versus its mass.

However, this estimate is consistent only with Earth-based vibrating screens, which are typically fabricated from steel. If titanium is considered as the primary construction material to reduce weight and increase resilience, the estimated mass decreases to approximately 2.57 tons. This represents a conservative approximation, as no auxiliary systems, actuators, or supports were included.

The Space Launch System (SLS) Block 1 Cargo has a launch capability to the Trans Lunar Injection orbit of 27 tons. Thus, even after allocating 2.6 tons for a vibrating screen, sufficient capacity (24 tons) remains available for additional cargo and landing systems. This suggests that lunar deployment of such equipment is logistically feasible.

A preliminary estimation was performed regarding power consumption. Assuming the mass calculated earlier, the natural frequency is lower than the operational frequency, the vibration amplitude is 0.5 mm, the operational frequency is 15 Hz, and a damping factor of 0.5, the required unbalanced force is about 14 kN. From manufacturer datasheets of the motovibrators, the required power to operate the vibrating screen is approximately 1.5 kW. Assuming photovoltaic supply, a solar panel area of 15 m² would be required (excluding storage and lunar day/night intermittency).

DISCUSSION

It is known that fine particles can clog a vibrating screen. Although this study did not show evidence of particles sticking to the mesh, clogging is likely under lunar conditions due to longer particle residence times and reduced stratification. Furthermore, due to the effect of electrostatic charges (Colwell *et al.* 2007; Nitano *et al.* 2025), lunar regolith strongly tends to adhere to screen surfaces and walls. Ultrasonic vibrations have been proposed and experimentally shown to be an effective solution to mitigate adhesion and clogging (Cannon *et al.* 2022; Kawamoto *et al.* 2011; Zanon *et al.* 2023).

Preliminarily, transport and implementation missions are not discarded, as mass requirements appear compatible with the SLS Block 1 Cargo capacity. Nevertheless, it is necessary to study the wear produced by the regolith on the screen to estimate spare parts requirements and ensure long-term operability. In addition, trommel screens should be investigated as an alternative, since their rotational motion may mitigate gravity dependence and address some of the kinematic challenges identified for vibrating screens under lunar gravity.

CONCLUSION

From the double-deck vibrating screen simulation, marked operational differences were observed between Earth and lunar conditions, resulting in a lower efficiency of the Moon screening process compared to the same configuration on Earth in most cases, as expected. Of the three studied variables, amplitude, frequency, and inclination, all three showed an increase in the process efficiency by lowering their values, with the vibration amplitude exerting the most decisive influence. Interestingly, the lunar cases outperformed Earth cases at lower amplitudes (e.g., 3 mm), suggesting a non-intuitive amplitude efficiency relationship under reduced gravity.

By using the auxiliary variable of the throwing index, higher efficiencies were expected by matching the lunar screen configuration to the best Earth-based case. However, contrary to expectations, the highest lunar efficiency was achieved with a configuration corresponding to a lower value. This indicates that , while useful on Earth, may not be directly transferable as a comparative metric across different gravitational environments, and further research is needed to redefine or adapt this parameter for extraterrestrial applications.

The best efficiency value obtained was 76.9%, which remains modest relative to efficiencies greater than 90% desirable to minimize energy use and accelerate resource preparation for future lunar infrastructure. Future studies will have to be conducted with lower amplitude values, , or alternative excitation geometries (e.g., elliptical or circular motions) to explore pathways toward higher efficiencies.

Numerical simulations, such as those performed here with DEM, represent a cost-effective tool for designing and planning lunar mining because they eliminate the immediate need for prohibitively expensive terrestrial or space-based experiments. Combined with complementary numerical models and targeted experimental validation, DEM provides a critical first step toward the integrated design of future lunar regolith processing plants.

CONFLICTS OF INTEREST

Nothing to declare.

AUTHOR CONTRIBUTIONS

Conceptualization: Lopez-Telgie A, Rodríguez C, and Moncada M; **Methodology:** Moncada M; **Software:** Cáceres P and Moncada M; **Validation:** Cáceres P, Lopez-Telgie A, Rodríguez C, Vicuña C, and Moncada M; **Formal analysis:** Rodríguez C and Vicuña C; **Investigation:** Cáceres P; **Resources:** Rodríguez C and Moncada M; **Data Curation:** Rodríguez C, Vicuña C, and Moncada M; **Writing - Original Draft:** Cáceres P and Moncada M; **Writing - Review & Editing:** Vicuña C and Moncada M; **Visualization:** Moncada M; **Supervision:** Lopez-Telgie A and Rodríguez C; **Project administration:** Lopez-Telgie A and Moncada M; **Funding acquisition:** Rodríguez C and Moncada M; **Final approval:** Moncada M.

DATA AVAILABILITY STATEMENT

The data will be available upon request.

FUNDING

Powered@SouthernGPU: this research was partially supported by the supercomputing infrastructure of the Southern GPU Cluster-Fondequip EQM150134.

DECLARE IF IA TOOLS WERE USED OR ADOPT

The authors declare that no artificial intelligence tools were used in the preparation, writing, data analysis, or review of this manuscript.

ACKNOWLEDGEMENTS

We acknowledge ESSS Group S.A. for the research license for this project within the framework of the strategic linkage with the Department of Mechanical Engineering of the University of Concepcion.

REFERENCES

Adachi M, Moroka HK, Wakabayashi S, Hoshino T (2017) Particle-size sorting system of lunar regolith using electrostatic traveling wave. J Electrostat 89:69-76. https://doi.org/10.1016/j.elstat.2017.08.002

Aghlmandi AA, Caner Orhan E, Levent Ergun S (2018) Discrete element modelling of vibrating screens. Miner Eng 121: 107-121. https://doi.org/10.1016/j.mineng.2018.03.010

Cannon KM, Dreyer CB, Sowers GF, Schmit J, Nguyen T, Sanny K, Schertz J (2022) Working with lunar surface materials: review and analysis of dust mitigation and regolith conveyance technologies. Acta Astronaut 196:259-274. https://doi.org/10.1016/j.actaastro.2022.04.037

Coetzee C (2019) Particle upscaling: calibration and validation of the discrete element method. Powder Technol 344:487-503. https://doi.org/10.1016/j.powtec.2018.12.022

Colwell J, Batiste S, Horányi M, Robertson S, Sture S (2007) Lunar surface: dust dynamics and regolith mechanics. Rev Geophys 45:RG2006. https://doi.org/10.1029/2005RG000184

Crawford IA (2015) Lunar resources: a review. Prog Phys Geogr Earth Environ 39:137-167. https://doi.org/10.1177/0309133314567585

Cundall PA, Strack OD (1979) A discrete numerical model for granular assemblies. Géotechnique 19(1):47-65. https://doi.org/10.1680/geot.1979.29.1.47

Dreyer CB, Walton O, Riedel EP (2012) Centrifugal sieve for size-segregation and beneficiation of regolith. Paper presented 2012 Earth and Space 2012: Engineering, Science, Construction, and Operations in Challenging Environments. ASCE; Pasadena, USA. https://doi.org/10.1061/9780784412190.004

[ESSS] Engineering Simulation and Scientific Software (2020) *Rocky 4.4 DEM technical manual.* Florianópolis: Brazil.

He X, Liu C (2009) Dynamics and screening characteristics of vibrating screen with variable elliptical trace. Min Sci Technol 19:508-513. https://doi.org/10.1016/S1674-5264(09)60095-8

Isachenkov M, Chugunov S, Akhatov I, Shishkovsky I (2021) Regolith-based additive manufacturing for sustainable development of lunar infrastructure – an overview. Acta Astronaut 180:650-678. https://doi.org/10.1016/j.actaastro.2021.01.005

Kawamoto H, Uchiyama M, Cooper B, McKay D (2011) Mitigation of lunar dust on solar panels and optical elements utilizing electrostatic traveling-wave. J Electrostat 69:370-379. https://doi.org/10.1016/j.elstat.2011.04.016

Li C, Zuo W, Wen W, Zeng X, Gao X, Liu Y, Ouyang Z (2021) Overview of the Chang'e-4 mission: opening the frontier of scientific exploration of the lunar far side. Space Sci Rev 217(35). https://doi.org/10.1007/s11214-021-00793-z

Li Z, Si Q, Jia P, Xiao G, Tong X (2023) Research on particle swarm screening mechanism and performance optimization based on simulated lunar microgravity. Adv Space Res 73(4). https://doi.org/10.1016/j.asr.2023.01.063

Lommen S, Schott D, Lodewijks G (2014) DEM speedup: stiffness effects on behavior of bulk material. Particuology 12: 107-112. https://doi.org/10.1016/j.partic.2013.03.006

McKay DS, Heiken G, Basu A, Blnford G, Steven S, Reedy R, Papike J (1991) The lunar regolith. Cambridge: Cambridge University. In: Lunar sourcebook; p 285-356.

Moncada M, Rodríguez C (2018) Dynamic modeling of a vibrating screen considering the ore inertia and force of the ore over the screen calculated with discrete element method. *Shock Vib* 2018:1-13. https://doi.org/10.1155/2018/1714738

Nitano R, Yamato S, Tanaka K, Kanamori H, Adachi M (2025) Cleaning performance of an electrodynamic dust shield under low-frequency vibrations. Powder Technol 457:120845. https://doi.org/10.1016/j.powtec.2025.120845

Otto H, Kerst K, Roloff C, Janiga G, Katterfeld A (2018) CFD-DEM simulation and experimental investigation of the flow behavior of lunar regolith JSC-1A. *Particuology* 36:164-177. https://doi.org/10.1016/j.partic.2017.12.003

Ozaki SI, Ishigami G, Otsuki M, Miyamoto H, Wada K, Watanabe Y, Nishino T, Kojima H, Soda K, Nakao Y, *et al.* (2023) Granular flow experiment using artificial gravity generator at International Space Station. npj Microgravity 9:61. https://doi.org/10.1038/s41526-023-00308-w

Pickrell J (2022) These six countries are about to go to the Moon – here's why. Nature 605(7909):208-211. https://doi.org/10.1038/d41586-022-01252-7

Sanders GB, Larson WE (2013) Progress made in lunar in situ resource utilization under NASA's exploration technology and development program. J Aerosp Eng 26:5-17. https://doi.org/10.1061/(ASCE)AS.1943-5525.0000208

Toledo P, Moncada M, Ruiz C, Betancourt F, Rodríguez C, Vicuña C (2025) A review of the application of the discrete element method in comminution circuits. Powder Technol 121027. https://doi.org/10.1016/j.powtec.2025.121027

Walton OR, Braun RL (1986) Viscosity, granular-temperature, and stress calculations for shearing assemblies of inelastic, frictional disks. J Rheol 30(5):949. https://doi.org/10.1122/1.549893

Zanon P, Dunn M, Brooks G (2023) Current lunar dust mitigation techniques and future directions. Acta Astronaut 213: 627-644. https://doi.org/10.1016/j.actaastro.2023.09.031